Doping a Mott insulator in an Ising-Kondo lattice: Strange metal and Mott criticality

Wei-Wei Yang,[1] Yin-Xia Li,[1] Yin Zhong,[1,*] and Hong-Gang Luo[1,2]

[1]*School of Physical Science and Technology & Key Laboratory for Magnetism and Magnetic Materials of the MoE, Lanzhou University, Lanzhou 730000, People's Republic of China*

[2]*Beijing Computational Science Research Center, Beijing 100084, China*

(Received 3 March 2021; revised 11 October 2021; accepted 12 October 2021; published 27 October 2021)

Metallic quantum states coined strange metal (SM), with robust linear-T resistivity, have been widely observed in many quantum materials under strong electron correlations, ranging from high-T_c cuprate superconductors and organic superconductors to twisted multilayer graphene and $MoTe_2/WSe_2$ superlattices. Despite decades of intensive studies, the mystery of SM still defies any sensible theoretical explanation and has been a key puzzle in modern condensed matter physics. Here, we solve a doped Mott insulator model called an Ising-Kondo lattice, which includes static spin fluctuation. With Monte Carlo simulation, the Ising-Kondo lattice unambiguously exhibits SM phenomena accompanied with quantum critical scaling in observables, e.g., resistivity, susceptibility, and specific heat. A closer look at SM reveals the breakdown of Landau's Fermi liquid theory without any symmetry breaking, i.e., the violation of Luttinger theorem. Our paper reveals that the long-overlooked static fluctuations in literature may play an essential role in non-Fermi liquid behaviors in correlated electron systems.

DOI: 10.1103/PhysRevB.104.165146

I. INTRODUCTION

Metallic quantum states deviated from the prediction of Landau Fermi liquid (FL) theory have been widely observed in many quantum materials since the discovery of high-T_c cuprate superconductor [1–3]. Among these non-Fermi liquid (NFL) states, the strange metal (SM) with robust linear-T resistivity stands out due to its ubiquitousness in correlated superconductors, heavy fermion compounds and recently uncovered twisted multilayer graphene. Since in many cases of copper oxides the superconductivity emerges directly as an instability of the SM phase, it is believed that understanding the nature of SM should be the key step to solve the high-T_c problem in cuprates and to establish the general framework for NFL phenomena [1–13].

To attack SM, plenty of intriguing theoretical proposals are created wherein the aspect of doped Mott insulator (MI) due to Phil Anderson suggests a fruitful pathway culminated in classic SU(2) gauge field theory [1,14]. Unfortunately, the strong coupling nature of gauge theory hinders the correct solution of doped MI though the perturbative calculation does predict a linear-T behavior in resistivity [15,16]. Alternatively, recent progress on the doped Hubbard model armed with state-of-the-art dynamic-mean-field theory (DMFT) revisits the issue of doped MIs, concluding that the elusive SM behaviors are caused by the doping-driven Mott quantum criticality [17,18]. Furthermore, a determinant quantum Monte Carlo (QMC) simulation performed in finite clusters confirms SMs at high-T regimes [19]. In addition, recent research revealed the violation of the Luttinger theorem in several typical strongly correlated electron models, e.g., the spinless $t-V$ model, the $t-J$ model, and also the Hubbard model, which unambiguously suggests doping the correlation-driven insulator/MI leads to the breakdown of Landau FL [19–28].

However, we have to emphasize that the mystery of SM has not been demystified due to the following reasons: (1) Since nonlocal spatial fluctuation, which is important in quantum criticality, has been greatly neglected in DMFT, the Mott criticality-driven SM phenomena may be fragile when spatial fluctuations are recovered [17,18]. (2) The QMC study only establishes the existence of SM at rather high-T ($T \sim t$) while the fate of SM at physically more relevant low-T regime ($T \ll t$, relevant to realistic experiments) has not been clarified due to the notorious fermions minus-sign problem in QMC [19]. (3) Even though the Hubbard model has been carefully examined, however, models besides Hubbard are also crucial to the understanding of many-bands systems like heavy fermion compounds [29–31].

Motivated by the aforementioned important progress and unsolved issues, in this paper we seek a clear and complete understanding about SM behaviors in doped MI with the help of an alternative model, which allows for nearly complete numerical treatment. Our departure is the doped Ising-Kondo lattice (IKL) model, which naturally mimics the strongly correlated f-electron materials CeIrSn [32], TmB_4 [33], hidden order compound URh_2Si_2 [34] and, at the same time, could be simulated by the unbiased Monte Carlo methods.

In this solid platform, we find that the competition between local and itinerant tendency leads to a rich phase diagram (the schematic phase diagram in Fig. 1) and reveals the desirable nontrivial SM physics. The macroscopic anomalies of SM are observed, which include the robust nonsaturating, T-linear resistivity and the logarithmic temperature dependence of specific-heat coefficient. Such exotic SM behaviors beyond

*zhongy@lzu.edu.cn

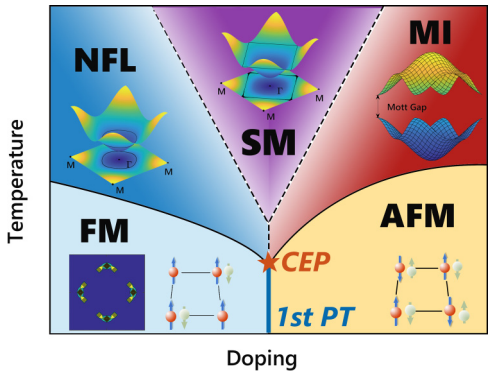

FIG. 1. Schematic phase diagram of the hole-doped Ising-Kondo lattice (IKL) model. The low-temperature regime is divided into an antiferromagnetic insulator (AFMI) and a ferromagnetic metal (FMM) by a first-order transition, which transforms to a weak first-order transition and finally ends at the critical end point (CEP). At high temperature above CEP, a quantum critical region (QCR) is induced by doping-driven Mott insulator-metal transition, which displays the strange metal (SM) behaviors. Out of QCR, there exists a Mott insulator (MI) at lower doping and a non-Fermi liquid (NFL) at a higher doping. Inset in MI shows two-band structure active at strong coupling while only lower band is depicted for SM and NFL.

the Landau's quasiparticle paradigm turn out to be intrinsically connected with the quantum criticality, which has also been observed in the vicinity of the quantum critical point (QCP) in various quantum critical heavy electron materials [4]. We also find that the absence of a quasiparticle picture is clearly indicated by a strong violation of Luttinger theorem throughout the paramagnetic regime in our model's finite-T phase diagram.

The remainder of this paper is organized as follows: In Sec. II, the IKL model is introduced and its phase diagram is briefly discussed. In Sec. III, the SM state is demonstrated by the calculation of resistivity and specific heat. The quantum critical scaling is also shown in this section. In Sec. IV, we show that the Luttinger theorem is violated in the IKL in terms of direct numerical calculation. Finally, Sec. IV gives a discussion on the relation of the IKL to the other models and ends with a summary.

II. MODEL AND PHASE DIAGRAM

We consider the IKL model on square lattice whose Hamiltonian is defined as

$$\hat{H} = -t\sum_{i,j\sigma}\hat{c}^{\dagger}_{i\sigma}\hat{c}_{j\sigma} + \frac{J}{2}\sum_{j\sigma}\hat{S}^{z}_{j}\sigma\hat{c}^{\dagger}_{j\sigma}\hat{c}_{j\sigma} - \mu\sum_{j\sigma}\hat{c}^{\dagger}_{j\sigma}\hat{c}_{j\sigma}, \quad (1)$$

where $\hat{c}^{\dagger}_{j\sigma}(\hat{c}_{j\sigma})$ is c electron's creation (annihilation) operator with spin $\sigma = \uparrow, \downarrow$ at site j. $\hat{S}^{z}_{j}$ denotes the spin-1/2 localized moment. In the language of heavy fermions, the c electron corresponds to the conduction electron while the localized moment results from the low-energy multiple states of $4f$ or $5f$ electrons [34]. The t-term denotes the hopping integral and only nearest-neighbor hopping is considered for simplicity. J is the longitudinal Kondo coupling between the c electron and localized moment at the same site [Fig. 2(a)]. In our previous work [35], a MI has been established in a half-filled system ($\mu = 0$) in the strong coupling regime ($J/t \gg 1$), which has a clear gap in the single-particle density of states around the Fermi energy.

Considering some readers may not be familiar with the above IKL model, we emphasize that it can be seen as the anisotropic limit of the more familiar Kondo lattice model [35]. The general (anisotropic) Kondo lattice model is written as

$$\hat{H} = -t\sum_{i,j\sigma}\hat{c}^{\dagger}_{i\sigma}\hat{c}_{j\sigma} + \sum_{j}\left[J_{\perp}\left(\hat{S}^{x}_{j}\hat{s}^{x}_{j} + \hat{S}^{y}_{j}\hat{s}^{y}_{j}\right) + J\hat{S}^{z}_{j}\hat{s}^{z}_{j}\right] - \mu\sum_{j\sigma}\hat{c}^{\dagger}_{j\sigma}\hat{c}_{j\sigma}, \quad (2)$$

where the spin density of the c electron at the j site is described as $\hat{s}^{\alpha}_{j} = \sum_{\sigma\sigma'}\hat{c}^{\dagger}_{j\sigma}\frac{\sigma^{\alpha}_{\sigma\sigma'}}{2}\hat{c}_{j\sigma'}$ with $\alpha = x, y, z$. $J_{\perp}, J$ are the transverse and longitudinal Kondo couplings, respectively. Now, we realize that in the limit $J_{\perp}/J = 0$, the above Kondo lattice reduces to the IKL as expected.

Inspired by the general consensus that doping the undoped MI would give rise to SM behavior, in this paper, we dope the half-filled IKL system and focus on the hole doping case by tuning the chemical potential μ. Since it is straightforward to translate the results in the hole-doping case to the electron-doping one, the latter will not be explicitly studied in this paper.

The method of choice for solving our IKL model Eq. (1) is the classical Monte Carlo simulation, which has been successfully used in the famous Falicov-Kimball model [36]. For the IKL, we observe that $[\hat{S}^{z}_{j}, \hat{H}] = 0$, thus the local moment $\hat{S}^{z}_{j}$ at each site is conserved. Then, if we choose eigenstates of $\hat{S}^{z}_{j}$ as basis, Eq. (1) will reduce into an effective free fermion model under fixed background $\{q_j\}$, ($q_j = \pm 1$, $\hat{S}^{z}_{j}|q_j\rangle = \frac{q_j}{2}|q_j\rangle$) thus permits a straightforward classical (lattice) Monte Carlo simulation. The detailed algorithm of the Monte Carlo simulation for IKL can be found in the Supplemental Material of our previous work [35].

Here, the Monte Carlo simulations of the IKL are carried out on the square lattice with periodic boundary conditions, where a 20×20 square lattice is mainly used. Accordingly, the two-dimensional Brillouin zone is sampled by a 20×20 k-point grid. The nearest-neighbor hopping integral is used as the unit ($t = 1$) to measure all energy scales. To attack the Mottness, we focus on the strong coupling regime ($J = 14$) [35].

In the IKL model, the competition between itinerant and local tendency leads to different magnetic orders, and thus further conspire to construct rich quantum states, including antiferromagnetic insulators (AFMIs), ferromagnetic metal (FMM) at low temperature, and paramagnetic phases as MI, SM, NFL at high temperature [Fig. 2(b)]. The AFMI state has finite checkerboard order and the Fermi energy is just located in the gap, while the FMM state has finite ferromagnetic order and the density of states is finite around the Fermi energy. The magnetic-paramagnetic phase transition [Fig. 2(b), purple line with circle] is determined by the peak in heat capacity [see Fig. 2(d)] and belongs to the two-dimensional Ising universality class, which is similar to the half-filled IKL [35]. There is

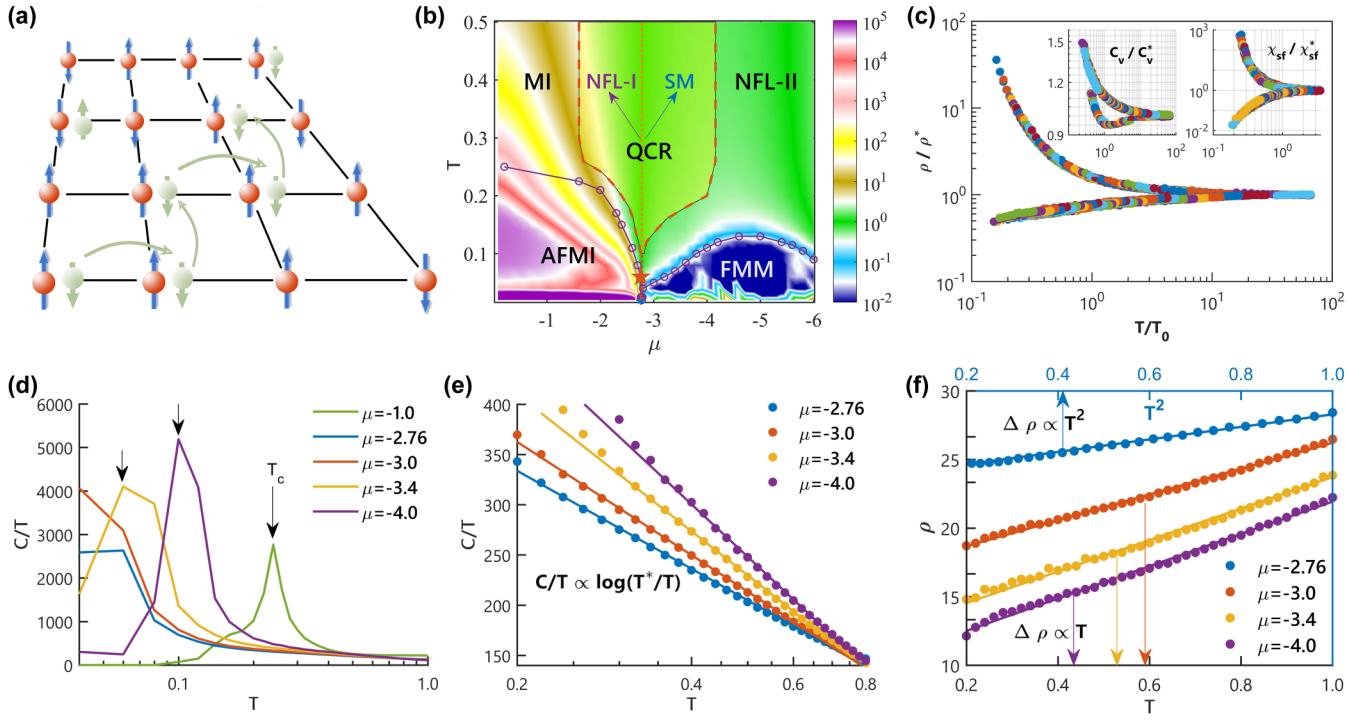

FIG. 2. Schematic picture, phase diagram of IKL, and SM behaviors in QCR. (a) Schematic representation of the doped IKL. (b) Phase diagram of the doped IKL model on square lattice in $\mu - T$ plane with $J = 14$. Rich quantum states include AFMI, FMM, MI, insulatorlike non-Fermi liquid (NFL-I), SM, and the second non-Fermi liquid (NFL-II). The background is a color map of the resistivity. Thermal fluctuation-driven magnetic-paramagnetic phase transition is denoted by the purple line with circle mark. The first-order phase transition at ground state is marked by a blue asterisk. The CEP is marked by a red pentagram. The QCR is delimited by the crossover temperature (red dashed line). (c) Unconventional quantum scaling behavior of resistivity in the QCR. Family of resistivity curves are calculated along lines parallel to the separatrix $\mu^*(T)$ and all can be rescaled in the formula $\rho(T, \delta\mu)/\rho^*(T) = f(T/T_0(\delta\mu))$. Inset plots the quantum scaling behavior of thermodynamic properties, i.e., heat capacity C_v of c electron and the susceptibility of f electron χ_{sf}. (d)–(f) Anomalous transport and thermodynamics in the SM. (d) Specific heat under different dopings. The peak position corresponds to T_c of magnetic-paramagnetic phase transition. (e) The same plot of specific heat in paramagnetic region with the y axis magnified. In SM, $C(T)/T$ exhibits logarithm temperature dependence. The solid line is fitted by a $\log(T^*/T)$ function. (f) Resistivity under different dopings. In the QCR, $\rho(T)$ satisfies a power-law dependence of temperature ($\rho(T) = \rho_0 + AT^n$). With increasing doping, the resistivity changes from T^2-dependent behavior ($\mu = -2.76$) to a linear-T dependence ($\mu = -3.0, -3.4, -4.0$), indicating the SM behavior

a lack of quasiparticles in all high-temperature phases. In the metallic region, the NFL state is confirmed by the anomalous resistivity or capacity heat behavior, whereas the SM state is more particular to additionally show quantum criticality and a logarithmic temperature dependence of specific-heat coefficient.

There exists a critical end point [CEP, see the red pentagram in Fig. 2(b)], below which a first-order phase transition separates the IKL system into AFMI and FMM. Above CEP, a QCR with unusual quantum scaling behavior is uncovered. Our main result about the doped IKL is summarized in the $\mu - T$ phase diagram [see Fig. 2(b)], where the color bar denotes resistivity scaled by the one in the separatrix line (dotted line) of QCR. We also elaborate a phase diagram in the $n_c - T$ plane in Supplemental Material [37]. Although rich quantum states are uncovered, in the rest of the paper we will not further discuss the properties of AFMI, FMM, and MI states. More details about low-T magnetic states can be found in the Supplemental Material [37]. Next we will focus on the nontrivial properties of the SM state and the violation of Luttinger theorem.

III. STRANGE METAL AND QUANTUM CRITICAL SCALING

As we know, the SM state is a particular NFL state with nontrivial characteristics. The presence of the SM state could be ascertained by anomalous thermal and transport properties [5,6,38,39]. We plot the evolution of heat capacity $C(T)$ and resistivity $\rho(T)$ with varying doping in Figs. 2(d)–2(f). In the SM phase, the heat capacity coefficient $C(T)/T$ increases with decreasing temperature, exhibiting an obvious dependence proportional to $\log(T^*/T)$ before approaching the magnetic phase transition, where T^* is the cutoff temperature. As for resistivity, an obvious linear-T dependence is revealed, which is nonsaturating with increasing temperature.

It has been suggested that it is the quantum critical physics that leads to both linear-T resistivity and high-T_c superconductivity. In most heavy fermion materials, the linear-T resistivity is observed when tuning some external parameters like magnetic field and pressure to create the QCP [40–44]. In our model, even without explicit second-order/continuous quantum phase transition, canonical signatures of quantum criticality are uncovered in a fanlike region together with

the SM phase in various physical properties, including the resistivity, heat capacity, and the magnetic susceptibility. In Fig. 2(c), we plot the unconventional quantum scaling behavior of these transport and thermodynamic observables. As a whole, resistivity in the QCR [see Fig. 2(f)] demonstrates a power-law dependence of temperature, satisfying $\rho(T) = \rho_0 + AT^n$, and the n gradually changes from 2 to 1 as the crossover to SM is occurring [37]. Detailed study indicates the resistivity of QCR satisfies the following quantum critical scaling:

$$\rho(T, \delta\mu) = \rho^*(T) f(T/T_0(\delta\mu)), \tag{3}$$

where $T_0(\delta\mu) = c|\delta\mu|^{z\nu}$, $\delta\mu = \mu - \mu^*(T)$ and $\mu^*(T)$ is the critical zero-field trajectory corresponding to the separatrix line. $\rho^*(T)$ is calculated for $\mu = \mu^*(T)$ and $f(x)$ denotes the unknown scaling function. The resistivity on the separatrix is almost independent with temperature. Note that at high temperatures, the resistivity curves depend weakly on different parameters, while as temperature is reduced the critical line separates resistivity curves to two branches. These results are crosschecked by a DMFT study [37]. Here, we refer the insulatorlike branch to the first NFL state (NFL-I) and the metallic one to SM, respectively. Out of QCR, at the high temperature region with larger doping, we dub the NFL state without quantum scaling behavior as the second non-Fermi liquid (NFL-II) [37].

The resistivity curves in the QCR region display the bifurcating characteristic. Crossing the center line, there is a change in trend with varying temperature. Both branches display the power-law scaling $T_0(\delta\mu) = c|\delta\mu|^{z\nu}$ with the same exponents $z\nu = 1.25$, and $T_0(\delta\mu)$ vanishes as $\delta\mu \to 0$, indicating a quantum criticality instead of classical phase transition. As shown in Fig. 2(c), we reveal that the critical exponent for c electron $[(z\nu)_c = 1.25]$ is different from the one of the f electron $[(z\nu)_f = 0.55]$.

In previous DMFT studies of the Hubbard model, the separatrix line $\mu^*(T)$ (the so-called instability trajectory) is determined as the minimum of curvature of the free-energy functional, i.e., the so-called quantum Widom line [17,18]. However, this method is no longer feasible in our Monte Carlo simulation. Fortunately, existing theoretical and experimental studies have confirmed that the scaling behavior is not sensitive to the choice of $\mu^*(T)$ [18]. Therefore, in this paper we alternatively determine the separatrix by the minimum of error bar with varying doping at a specific temperature in Monte Carlo simulation to mark the states in equal proximity to both FMM and AFMI. The error bar is an appropriate quantity to determine the separatrix, which has an intrinsic dynamic feature. Since the minimum of error bar infers that the calculated quantity is least relevant to the magnetic configuration, thus it corresponds to the state with no more tendency to either competing phase. We carry out a careful Monte Carlo simulation and reveal the separatrix is located at $\mu = -2.76$ (denoted as red dotted line in all plots), which is almost independent upon variation of temperature.

IV. VIOLATION OF LUTTINGER THEOREM

Given the unconventional quantum criticality, it is natural to further examine the quasiparticle properties in the exotic SM phase. To this aim, we examine the validity of the Luttinger theorem in our model [45–48], which states that if Landau quasiparticle exists, the volume enclosed by the Fermi surface is consistent with its density of particles. Such theorem has been proved originally by Luttinger in terms of perturbation theory [46,47], and later by Oshikawa's nonperturbation topological argument [48]. It now has been accepted as a key feature of FL. Mathematically, Luttinger theorem means the Luttinger integral (IL) below must be equal to density of particles (n_c):

$$\mathrm{IL} = \sum_{\sigma} \int_{\theta(\mathrm{Re}G(\mathbf{k},\omega=0))} \frac{d^d k}{(2\pi)^d}. \tag{4}$$

Here, $G(\mathbf{k}, \omega)$ is the retarded single-electron Green's function and $\theta(x)$ is the standard unit step function with $\theta(x > 0) = 1$ and $\theta(x < 0) = 0$. For the lattice model with finite sites, the above momentum integral should be replaced by discrete summation. Frankly speaking, Eq. (4) is strictly valid only for zero temperature, however, interesting physics like SM or other NFLs often exist at finite-T. Here, we follow the recent QMC study on the doped Hubbard model in Ref. [21] and still use Eq. (4) to estimate the validity of Luttinger theorem at finite temperature. [Temperature effect seems to be small at high-T regime, see, e.g., Fig. 3(a)].

Interestingly, according to our Monte Carlo data, we see the whole high-temperature region of the IKL violates the Luttinger theorem heavily. The strong violation of the Luttinger theorem is demonstrated in Fig. 3(a), which is robust with arbitrary doping for the strong coupling ($J = 14$, IL $> n_c$). It suggests a robust NFL-like nature for all paramagnetic phases in the phase diagram [see Fig. 2(b)], including SM. As a reference, we also show that the Luttinger theorem works well in the weak coupling case ($J = 2$, IL $\sim n_c$), agreeing with its FL nature. The extra feature in Fig. 3(a) is that the IL shows incipient divergence around $n_c \sim 0.53$, which is close to the boundary of QCR.

The violation of Luttinger theorem could be characterized clearly by the c electron's single-particle spectral properties. As shown in Fig. 3(b), the c electron's spectral function $A_{\mathbf{k}}(\omega = 0)$ and the real part of Green's function $\mathrm{Re}G(\mathbf{k}, \omega = 0)$ at Fermi energy are carefully studied. We compare the IL and electron density in FL (left panel), SM (middle panel), and NFL-II (right panel).

According to Luttinger theorem, electron density can be denoted by the size of the Fermi surface's volume in the free system. In Fig. 3(b), we use the white line to mark such a Fermi surface for the free system. It shows nicely and clearly the working of the Luttinger theorem for the FL. Under weak coupling, the volume enclosed by the Fermi surface is consistent with the one in the free system ($n_c = 0.36$). It suggests the presence of a quasiparticle, which means the correspondence between interacting and noninteracting c electrons is valid, since in this weak coupling situation the volume enclosed by the Fermi surface has not changed due to interaction. To the contrary, both the SM ($n_c = 0.67$) and NFL-II ($n_c = 0.31$) states display violation of Luttinger theorem, where the electron density is deviated from the volume enclosed by the Fermi surface, underlying the destruction of the quasiparticle in the paramagnetic regime of the doped IKL.

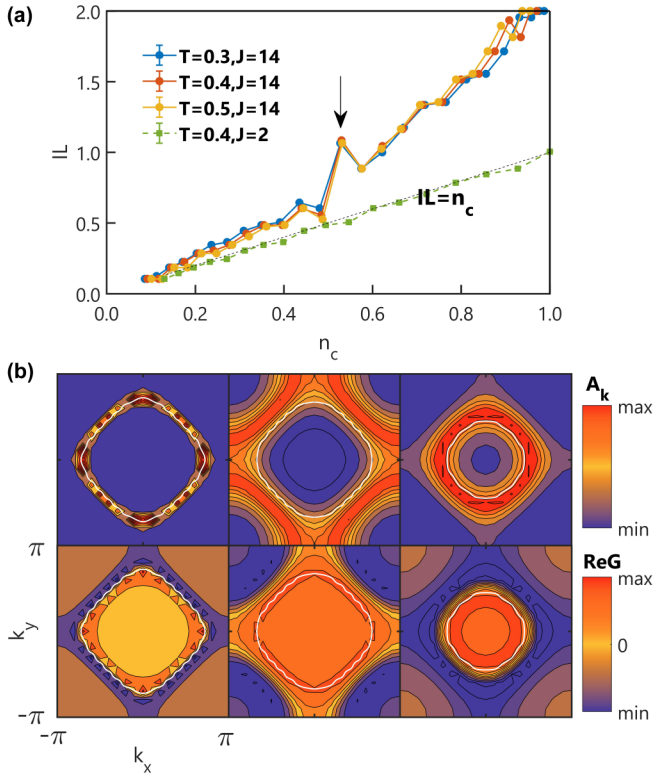

FIG. 3. Violation of Luttinger theorem. (a) Luttinger integral (IL) versus density of electron n_c. In FL ($J = 2$), the electron density is in accordance with the Luttinger theorem. At strong coupling ($J = 14$), IL strongly deviates from the density of electron for most doping regimes, thus confirming its NFL nature. IL diverges close to the boundary of QCR. Divergence is indicated by the arrow. (b) Spectral function at Fermi energy $A_{\mathbf{k}}(\omega = 0)$ (upper panel) and real part of Green's function at Fermi energy $\mathrm{Re}G(\mathbf{k}, \omega = 0)$ (lower panel) in different high-temperature phases: FL (left panel, $J = 2$, $T = 0.4$, $\mu = -0.8$), SM ($J = 14$, $T = 0.4$, $\mu = -3.0$, middle panel), NFL-II ($J = 14$, $T = 0.4$, $\mu = -4.6$, right panel). Electron density is denoted by the size of the Fermi surface's volume in a free system (white circle). The maximum of spectral function corresponds to the Fermi surface under strong coupling.

A careful reader may ask why physically SM and NFL show the violation of Luttinger theorem. Here, we provide a possible explanation. First, one may note that when J/t is large (e.g., $J = 14$), the single-particle density of states in SM and NFL shows a two-band structure just like the familiar upper and lower Hubbard subband in the Hubbard model (see Fig. 6 in the Supplemental Material [37] or in our previous paper Ref. [35]). In contrast, if $J = 0$, only one band exists as the free electron band. Then, the evolution from the one-band to two-band picture is not consistent with the correspondence between noninteracting and interacting electrons, which is the core idea of Landau's quasiparticle and the FL theory. Thus, the violation of Luttinger theorem is expected in SM and NFL, which are both paramagnetic states in doped MI.

V. DISCUSSION AND CONCLUSION

We remark that a similar phase diagram like Fig. 2(b) has been reported in the Hubbard model with the DMFT approximation [17,18]. Comparing the anomalous phenomena in the IKL and the Hubbard model, we find these two models share several common properties around MI-metal transition as follows. (i) A robust NFL state is revealed around the transition with a linear-T resistivity [e.g., Fig. 2(f)]. (ii) The Mott transition turns out to be third order, indicated by the divergence of $\frac{\partial^2 n_c}{\partial \mu^2}$. (iii) Resistivity satisfies a quantum critical scaling like Eq. (3) with a similar critical exponent $[(z\nu)_{\mathrm{IKL}} = 1.25, (z\nu)_{\mathrm{Hubbard}} = 1.35]$.

There also exist some differences. The doped MI in the IKL has a rigid band while in the Hubbard model spectral-weight transfer leads to a nonrigid band. Furthermore, our Monte Carlo simulation in the IKL includes both local and nonlocal correlation and, consequently, the low temperature phases of the IKL turn out to be magnetic ordered states. Even without QCP, the quantum scaling behavior is confirmed in this solid platform. However, the DMFT applied in the Hubbard model makes a strong approximation such that the magnetic orders are suppressed at low temperature. Considering multiple low-temperature competing orders are all neglected, the uncovered QCP and even the quantum critical behavior in DMFT study might be artificial.

Comparing the IKL to solvable doped MI in the Hatsugai-Kohmoto (HK) model [49], one can see that no Luttinger surface exists in the IKL (also in the Sachdev-Ye-Kitaev model and the Hubbard model) while the HK supports robust Luttinger surface characterized by zeros of Green's function. Thus, the Luttinger surface may not be a generic feature for doped MI though it does kill FL.

In conclusion, by studying a numerically solvable doped MI, exotic SM behaviors are revealed in the QCR, including the nonsaturating T-linear resistivity and the logarithmic temperature dependence of the specific-heat coefficient. These exotic behaviors elucidate the absence of quasiparticles, and it is further confirmed unambiguously by the violation of Luttinger theorem throughout the whole paramagnetic region of the phase diagram. Compared with the classic Hubbard model, our study suggests that SM, Mott quantum criticality, and the presence of Fermi surface are the intrinsic features of doped MI, which are promising to be revealed in generic strongly correlated electron systems.

ACKNOWLEDGMENTS

This research was supported in part by Supercomputing Center of Lanzhou University and NSFC under Grants No. 11704166, No. 11834005, No. 11874188, No. 11674139. We thank the Supercomputing Center of Lanzhou University for allocation of CPU time.

APPENDIX A: PHASE DIAGRAM WITH COMPRESSIBILITY

A similar phase diagram is also elaborated with color-coded compressibility, on both $T - \mu$ and $n_c - T$ plane (see Fig. 4) to provide a more intuitive insight into IKL. The MI state turns out to emerge in a quite small region with Fermi level in the band gap. Since in the band gap the particle number is not sensitive to the change of chemical potential, the MI region looks much larger in the $T - \mu$ phase diagram.

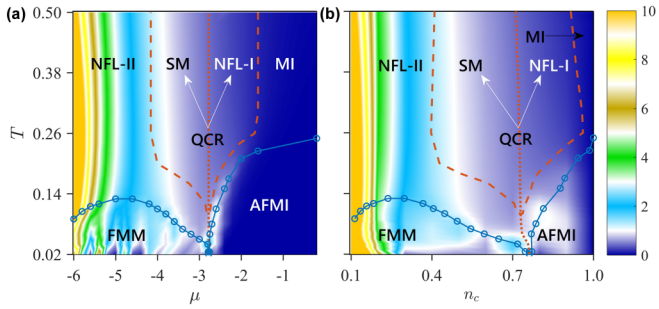

FIG. 4. Phase diagram of the doped IKL in the background of color-coded charge compressibility in (a) $\mu - T$ plane, (b) $n_c - T$ plane. The low-temperature regime is divided into an AFMI and a FMM by a first-order transition, which transforms to a weak first-order transition and finally ends at the CEP. At high temperature above CEP, a QCR is induced by doping-driven Mott insulator-metal transition, which displays the SM behavior in the metallic part. We refer the insulatorlike part to NFL-I. Out of QCR, there exists a MI at lower doping and the NFL-II at a higher doping.

Actually, as shown in Fig. 4(b), the SM behavior sustains within a quite wide range of doping.

APPENDIX B: DYNAMICAL MEAN-FIELD ANALYSIS

In this section, we cross-check the scaling behavior observed by Monte Carlo simulation with the single-site DMFT. Even without nonlocal correlations, the DMFT could still provide a completely nonperturbative description of the strong interaction effect. Especially at the high temperature where most nonlocal correlations are destroyed by thermal fluctuation, the DMFT is quite reliable. Its result could help identify the effect of insulator-metal crossover and exclude the influence of magnetic transition. The QCR is just located in the paramagnetic region and could be understood in the framework of DMFT.

In Figs. 5(a) and 5(b), we plot the scaling behavior of the resistivity curves parallel with the separatrix line. We report that the results obtained with Monte Carlo simulation and DMFT qualitatively agree with each other at $J = 14$. In both branches, the scaling parameters are chosen in the power-law form with the same exponents. The scaling holds in the doping region ($-0.04 \leqslant \delta\mu \leqslant 0.04$), which is very small due to the strong correlation. In addition, we note that a perfect mirror symmetry is revealed at all parameters. As in the analysis in previous studies [18], the authors provide a smart method to evaluate the exponent,i.e., in the systems with such remarkable mirror symmetry the resistivity curve along the separatrix could be fitting with exponent $z\nu$ as

$$\frac{\partial \log \rho^*(\mu, T)}{\partial \mu} \propto T^{-\frac{1}{z\nu}}. \tag{B1}$$

With this formula, we display a perfect fitting behavior in Fig. 5(c) and it does cover a quite large temperature scale. The exponent is fitted as $z\nu = 1$, which is applied in Fig. 5. The critical exponent in the DMFT $z\nu = 1$ indicates the scaling behavior might belong to the classical Ising universality class. What's more, the low-temperature

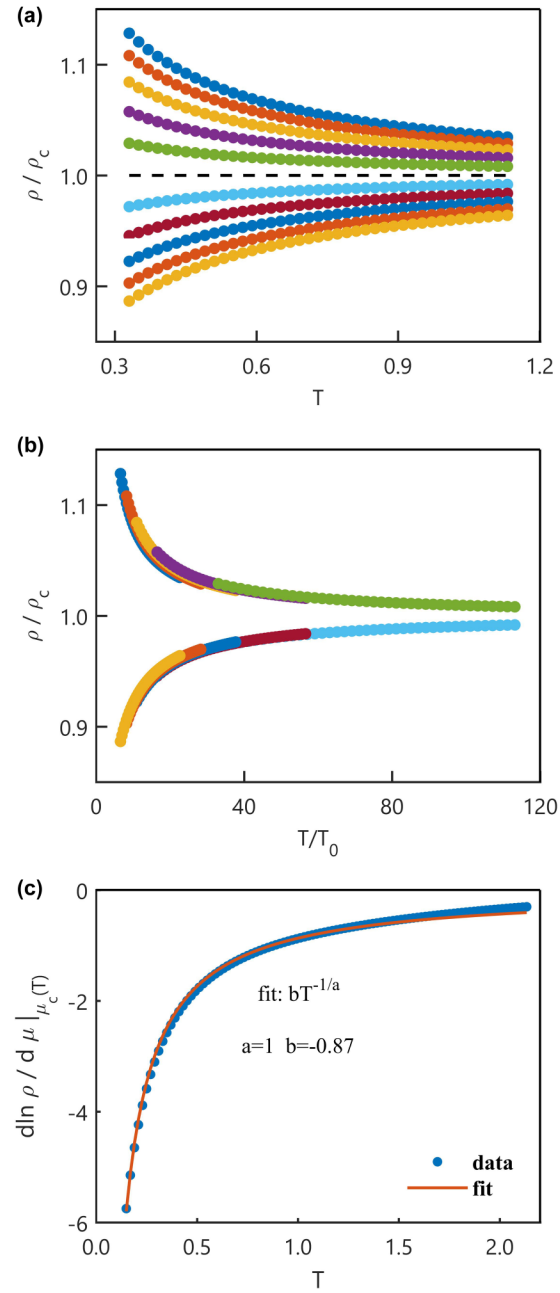

FIG. 5. (a) Resistivity curves calculated by dynamical mean field theory (DMFT), which are plotted along different trajectories $-0.04 \leqslant \delta\mu \leqslant +0.04$ with respect to the separatrix line (black dash line). (b) Scaling behavior of resistivity. (c) Derivative of resistivity with respect to μ ($\partial\rho(\mu, T)/\partial\mu|_{\mu_c}$) along the separatrix line. It fits well to a power-law curve with exponent -1, indicating the scaling formula exponent $z\nu = 1$.

magnetic transition emanated from the CEP also displays the standard classical liquid-gas universality class. This Ising scaling could be understood in the way that the phase diagram is mainly divided to two magnetic states, i.e., the FM one and the AFM one, and these two dominant phases as two whole parts compete with each other. Thus it leads to kinds of Ising-like criticality through the entire parameter region.

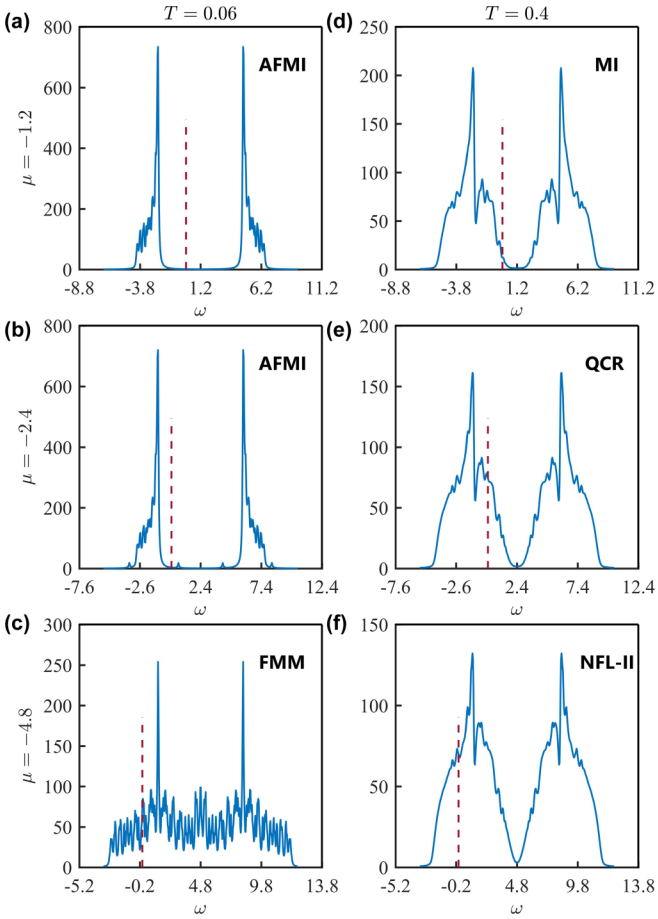

FIG. 6. Density of states (DOS) in low-temperature regions (left panel, $T = 0.06$) and high-temperature regions (right panel, $T = 0.4$). Position of Fermi level is marked with right dashed line.

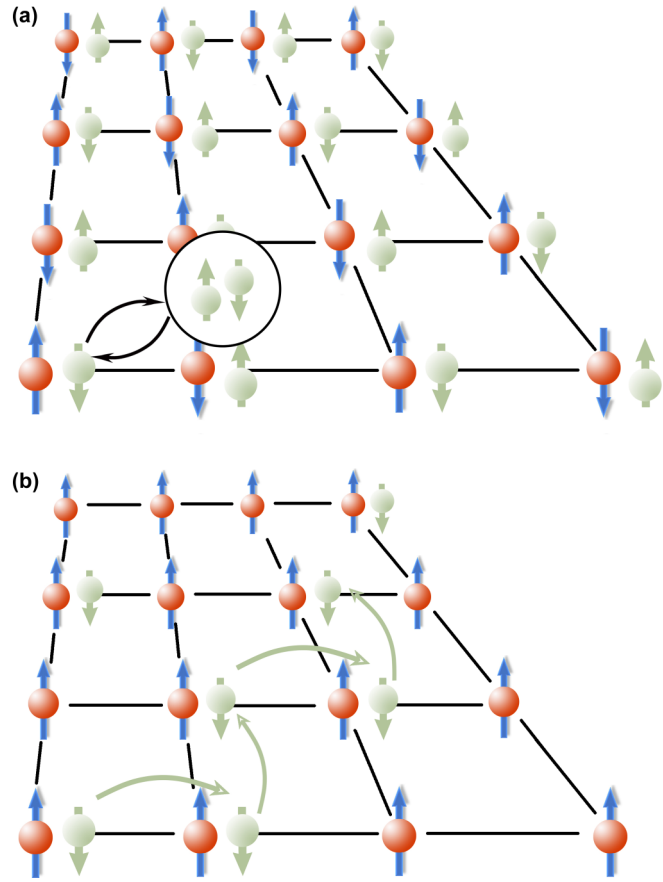

FIG. 7. Schematic explanation of the magnetic structure at different doping levels. f electrons are denoted by red balls, and itinerant electrons are denoted by green balls. (a) Around half filling, antiferromagnetic (AFM) configuration permits the virtual hopping of c electrons, leading to delocalization with lowered kinetic energy $E_0^{(2)} \sim -\frac{4t^2}{J}$. In the ferromagnetic (FM) background, the virtual hopping is instead forbidden by the Pauli exclusion principle. (b) Away from half filling, FM configuration could enhance the conductivity of c electrons, where c electrons could freely move in the FM background without the charge of energy elevation. To the contrary, electron movement would be hindered in the AFM configuration, since the spin orientations of c electron and its neighbor local moments are parallel to each other and thus hopping will greatly enhance the energy ($\Delta E \sim \frac{J}{4}$).

APPENDIX C: MAGNETIC STATES AT LOW TEMPERATURE

1. Magnetic states

In previous studies about the half-filling IKL [35], we confirm the theorem proved by Kennedy and Lieb [50] with Monte Carlo simulation, i.e., the ground-state configuration $\{q_i\}$ has the twofold degenerated checkerboard order $q_j = \pm(-1)^j$. In this paper, we report that, not only for the half-filling situation, at any doping level the IKL system always has a magnetic-ordered ground state. In addition, due to the strong longitudinal Kondo coupling, c electrons construct the same magnetism with local moments. In this section, we will illustrate the mechanism of each state and analyze transition properties between different states.

At the left side of CEP, as shown in Fig. 2(b), the $\{q_i\}$ has Néel AFM configuration. Around the half-filling situation, IKL is a MI with AFM order. With increasing doping, there is a crossover to the normal AFMI state. Further increasing doping holes leads to the FMM state, when across the CEP to its right side. We confirm different magnetic structures with a significant structure factor in the Brillouin zone. The insulating and metallic states are confirmed by the behavior of DOS and resistivity. In the left panel of Fig. 6, we demonstrate the DOS at different doping levels. The zero DOS($\omega = 0$) at small doping and finite DOS($\omega = 0$) at large doping suggest a transition from insulator to metal. AFMI is characterized by a fully open gap and increasing resistivity with decreasing temperature. In the FMM state, it instead has finite DOS($\omega = 0$) and the resistivity decreases with decreasing temperature. In Fig. 6(c), (left panel), the clear quasiparticle peak suggests a FL-like behavior. Even at the metallic state ($\mu = -5, -6$), resistivity still has an upward tendency at sufficiently low temperature, which is attributed to the weak localization property of a two-dimensional system.

The mechanism of different magnetism at small and large dopings is illustrated in Fig. 7, respectively. Under strong interaction, the Kondo coupling term could be taken as the zero-order Hamiltonian while the hopping term is merely taken as perturbation. Due to strong correlation, double occupation would significantly elevate the energy and give the

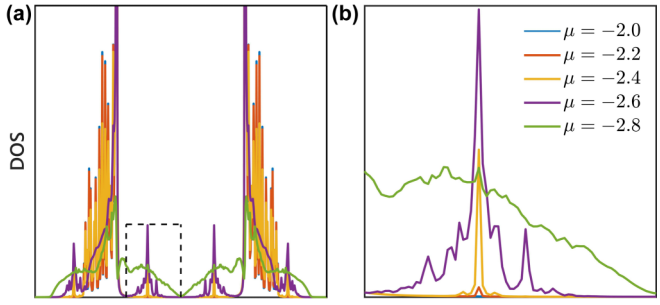

FIG. 8. DOS calculated at $T = 0.06$ at different levels of doping. For clarity, we adjust the x axis ω to unify the location of gap in different curves.

energy change $\Delta E \sim \frac{J}{4}$, thus c electrons can hardly move on lattice. Therefore, around half filling, the ground state is insulating, where c electrons localized at each site ($n_c \precsim 1$). The tendency from antiferromagnetism to ferromagnetism with increasing doping can be understood under the framework of perturbation theory. In antiferromagnetism, the process of virtual hopping of c electrons leads to delocalization and thus decreases the kinetic energy [$E_0^{(2)} \sim -\frac{4t^2}{J}$, see Fig. 7(a)]. This mechanism is similar to the one in the half-filled Hubbard model [51]. As to large doping, the lattice is away from half filling and hopping of c electrons is no longer forbidden. Thus the charge transport would be hindered by the presence of an AFM background, whereas the FM background can greatly enhance the conductivity. (In the AFM background, spin of c electron would be antiparallel to the on-site local moment, whereas parallel to the nearest-neighbor local moment.) Thus, with increasing doping the delocalization of c electrons occurs together with a magnetic-structure transformation, leading to a FMM state.

Actually, before approaching the AFMI-FMM phase transition, the competition between different magnetic structures is already present and leads to spin excitations. In Fig. 8, we display the DOS around the transition in the AFMI state. When exceeding a critical doping (around $\mu = -2.2$), a bound state emerges in the fully opened Mott gap. The bound state is caused by the domain-wall excitation of an AFM configuration in the parameter region away from half filling. It is the lead up to the magnetic phase transition.

2. Magnetic phase transition

The transition property of IKL is complicated, which combines the competing between both metal-insulator and AFM-FM structures. As shown in the main text, at ground state the AFM-FM transition occurs around $\mu_c = -2.76$ and is a strong first-order phase transition (marked by a blue asterisk). In Fig. 9, we plot the finite-size scaling behavior of checkerboard order parameter ϕ_c to investigate the transition properties. In a small doping region ($-2.80 \leqslant \mu \leqslant -2.74$), the checkerboard order parameter and the c-electron density ($n_c \sim 0.76$) are almost invariant [see Fig. 9(a)]. This suggests a strong first-order phase transition located along a coexistence dome, which includes the spin density wave states with (0,0), (π, π), $(\pi, 0)$, $(0, \pi)$ order. The coexistence regime would be much larger under a weak correlation. Increasing

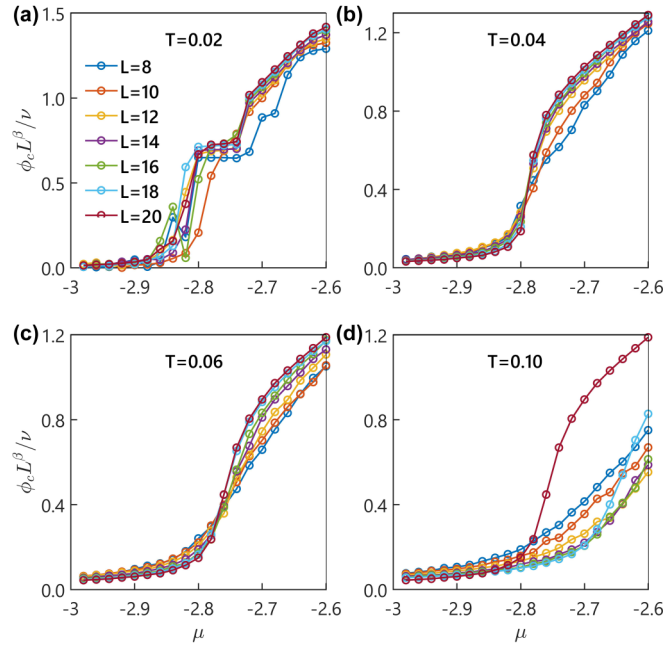

FIG. 9. Finite-size scaling behavior of checkerboard order parameter ϕ_c for different temperatures (a) $T = 0.02$, (b) $T = 0.04$, (c) $T = 0.06$, (d) $T = 0.10$. At sufficiently low temperature (a), the flat order parameter suggests a first-order phase transition, along with the coexistent region of antiferromagnetism and ferromagnetism. The crossing of the different system sizes at T_c reveals a scaling behavior belongs to a 2D Ising universality class at (b), (c), suggesting a weak first-order phase transition. At higher temperature (d), the scaling behavior vanishes, instead indicating a crossover or phase transition in higher order.

temperature leads to a weak first-order phase transition. In Figs. 9(b) and 9(c), the finite-size scaling behavior, which belongs to the two-dimensional Ising universality class, indicates a weak first-order phase transition. This phase transition finally terminates at the CEP ($T = 0.06$, $\mu = -2.76$). Further

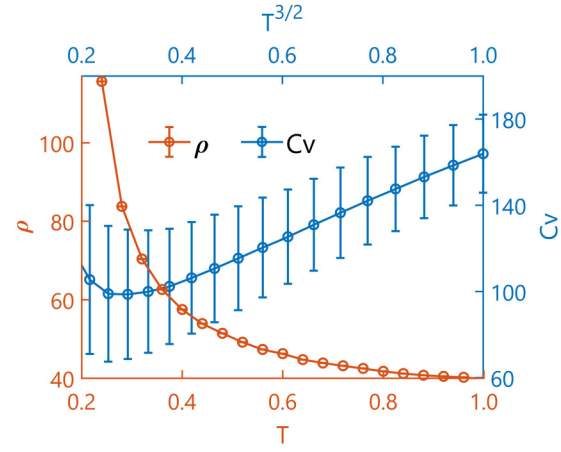

FIG. 10. Anomalous transport and thermodynamics in the first non-Fermi liquid state (NFL-I, $\mu = -2.0$), which is the insulatorlike part of the QCR. Specific heat (orange) displays a $T^{3/2}$ dependence at high-temperature region, which is out of the FL paradigm. The resistivity (blue) increases with decreasing temperature, indicating insulatorlike transport properties.

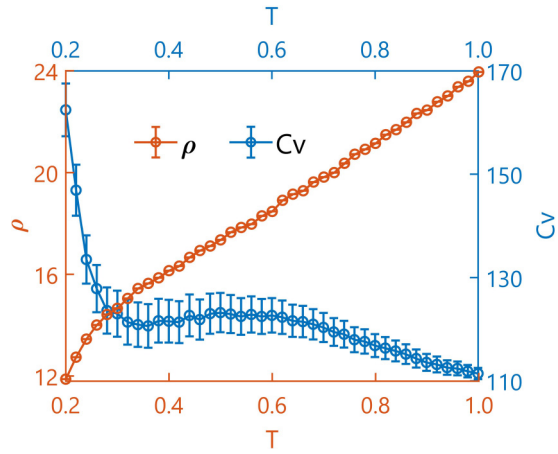

FIG. 11. Anomalous transport and thermodynamics in the second non-Fermi liquid state (NFL-II, $\mu = -4.6$), which is the high temperature region out of the QCR. The resistivity (blue) displays an obvious linear-T dependence.

increasing the temperature, a metal-insulator crossover occurs instead [see Fig. 7(d)].

APPENDIX D: NON-FERMI LIQUID STATES AT HIGH TEMPERATURE

As shown in Fig. 4, there are four different states at high temperature: MI, NFL-I, SM, and NFL-II. With increasing temperature, an obvious transformation of DOS occurs with the thermally driven magnetic-paramagnetic phase transition. At high temperature, the two-peaked spectral function is

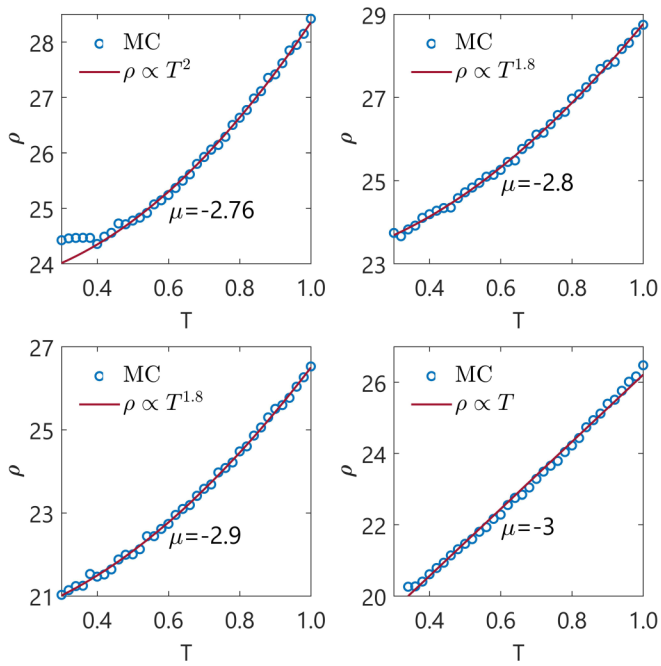

FIG. 12. Resistivity around the crossover from NFL-I to SM. The resistivity changes from T^2-dependent behavior to a linear-T dependence.

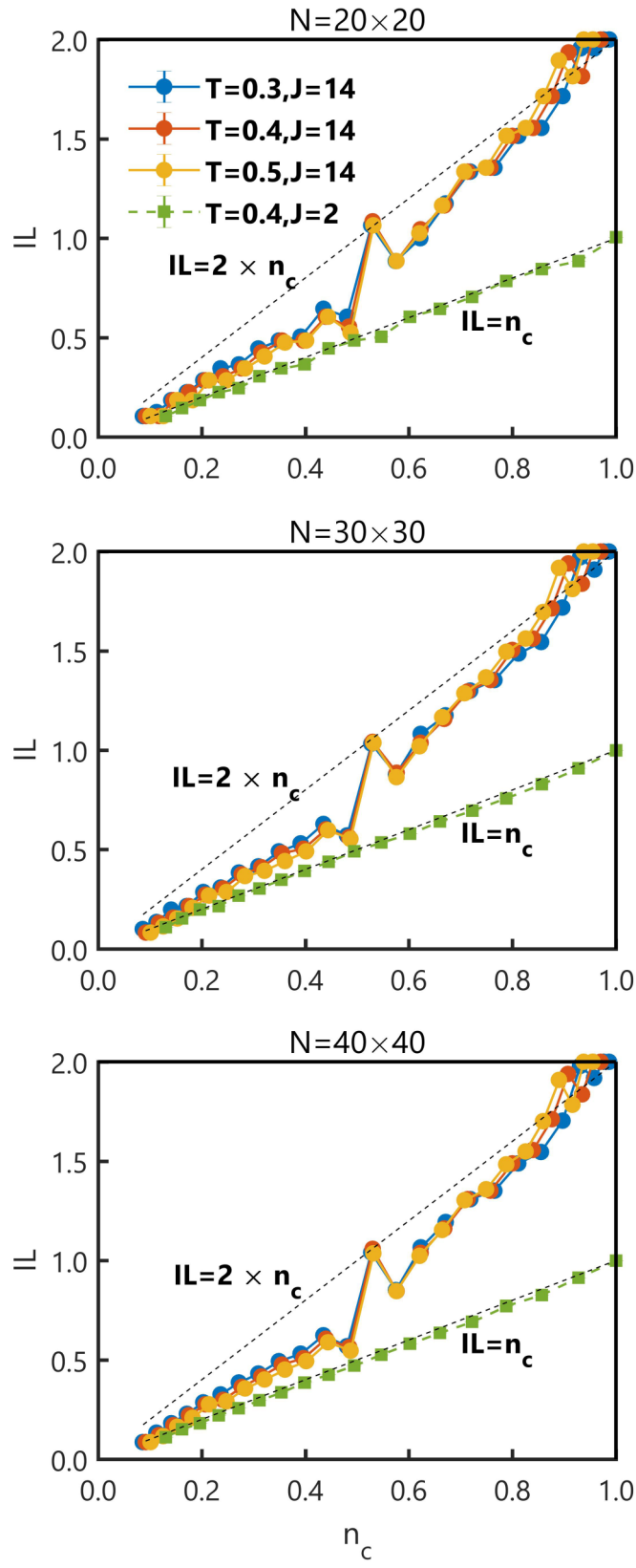

FIG. 13. Finite-size effect of the violation of the Luttinger theorem. The Luttinger integral is calculated in systems of different sizes ($N_s = 400, 900, 1600$).

robust (see the right panel of Fig. 6). Due to strong coupling, most paramagnetic region of doped IKL displays robust NFL behavior, which is indicated by the violation of Luttinger's theorem.

We refer the insulatorlike part of QCR to the NFL-I. In Fig. 10, we demonstrate the anomalous transport and thermodynamics of the NFL-I state ($\mu = -2.0$). In NFL-I, the capacity heat displays an obvious $T^{3/2}$ dependence, which is out of the FL paradigm. As shown in the main text, the resistivity curves display unconventional quantum scaling behavior. However, the insulating properties dominate in a quite large temperature region and thus the resistivity cannot be well scaled by T^{α}.

In Fig. 11, we demonstrate the anomalous transport and thermodynamics of the NFL-II, which is referred to as the large doping regime out of QCR. In the NFL-II a linear-T resistivity is revealed. We distinguish the NFL-II from SM by the absence of both quantum critical scaling behavior and logarithmic temperature dependence of the specific-heat coefficient.

The SM regime displays a T^n-dependence resistivity. Close to the crossover of NFL-I to SM, n changes from 2 to 1 gradually (see Fig. 12).

APPENDIX E: FINITE SIZE EFFECT OF VIOLATION OF LUTTINGER THEOREM

At high occupied situations, the Luttinger integral far deviates from n_c, where IL $\sim 2n_c$ is satisfied. When $n_c < 0.53$, the curves are closer to IL $= n_c$. Here we check the effect due to the finite size and the Luttinger theorem is discussed in systems of different sizes ($N_s = 400, 900, 1600$). As shown in Fig. 13, the deviation is robust although the value at small n_c is smaller than the high occupied situation. For strongly correlated systems, the Luttinger theorem is violated in the almost doping regime. On the contrary, at the weak coupling situation the Luttinger integral is exactly on the n_c curve ($J = 2$). This result is reasonable since the strong coupling induces robust two-peak spectral function with varying doping. The robust Mott gap destroys the quasiparticle picture.

[1] P. A. Lee, N. Nagaosa, and X.-G. Wen, Rev. Mod. Phys. **78**, 17 (2006).
[2] G. R. Stewart, Rev. Mod. Phys. **83**, 1589 (2011).
[3] B. J. Powell and R. H. McKenzie, Rep. Prog. Phys. **74**, 056501 (2011).
[4] B. Shen, Y. Zhang, Y. Komijani, M. Nicklas, R. Borth, A. Wang, Y. Chen, Z. Nie, R. Li, X. Lu, H. Lee, M. Smidman, F. Steglich, P. Coleman, and H. Yuan, Nature **579**, 51 (2020).
[5] R. Daou, N. Doiron-Leyraud, D. LeBoeuf, S. Y. Li, F. Laliberté, O. Cyr-Choinière, Y. J. Jo, L. Balicas, J.-Q. Yan, J.-S. Zhou, J. B. Goodenough, and L. Taillefer, Nat. Phys. **5**, 31 (2009).
[6] A. Legros, S. Benhabib, W. Tabis, F. Laliberté, M. Dion, M. Lizaire, B. Vignolle, D. Vignolles, H. Raffy, Z. Z. Li, P. Auban-Senzier, N. Doiron-Leyraud, P. Fournier, D. Colson, L. Taillefer, and C. Proust, Nat. Phys. **15**, 142 (2019).
[7] F. Kagawa, K. Miyagawa, and K. Kanoda, Nature **436**, 534 (2005).
[8] H. Oike, K. Miyagawa, H. Taniguchi, and K. Kanoda, Phys. Rev. Lett. **114**, 067002 (2015).
[9] S. S. P. Parkin, E. M. Engler, R. R. Schumaker, R. Lagier, V. Y. Lee, J. C. Scott, and R. L. Greene, Phys. Rev. Lett. **50**, 270 (1983).
[10] J. A. N. Bruin, H. Sakai, R. S. Perry, and A. P. Mackenzie, Science **339**, 804 (2013).
[11] J. Zaanen, SciPost Phys. **6**, 61 (2019).
[12] B. Keimer, S. A. Kivelson, M. R. Norman, S. Uchida, and J. Zaanen, Nature **518**, 179 (2015).
[13] J. Custers, P. Gegenwart, H. Wilhelm, K. Neumaier, Y. Tokiwa, O. Trovarelli, C. Geibel, F. Steglich, C. Pépin, and P. Coleman, Nature **424**, 524 (2003).
[14] P. W. Anderson, Science **235**, 1196 (1987).
[15] I. Affleck, Z. Zou, T. Hsu, and P. W. Anderson, Phys. Rev. B **38**, 745 (1988).
[16] X.-G. Wen and P. A. Lee, Phys. Rev. Lett. **76**, 503 (1996).
[17] J. Vučičević, D. Tanasković, M. J. Rozenberg, and V. Dobrosavljević, Phys. Rev. Lett. **114**, 246402 (2015).
[18] J. Vučičević, H. Terletska, D. Tanasković, and V. Dobrosavljević, Phys. Rev. B **88**, 075143 (2013).
[19] E. W. Huang, R. Sheppard, B. Moritz, and T. P. Devereaux, Science **366**, 987 (2019).
[20] L. D. Landau, Sov. Phys. JETP **3**, 920 (1957).
[21] I. Osborne, T. Paiva, and N. Trivedi, arXiv:2001.07197.
[22] J. Kokalj and P. Prelovšek, Phys. Rev. B **78**, 153103 (2008).
[23] W. O. Putikka, M. U. Luchini, and R. R. P. Singh, Phys. Rev. Lett. **81**, 2966 (1998).
[24] J. Kokalj and P. Prelovšek, Phys. Rev. B **75**, 045111 (2007).
[25] J. Schmalian, M. Langer, S. Grabowski, and K. H. Bennemann, Phys. Rev. B **54**, 4336 (1996).
[26] C. Gröber, R. Eder, and W. Hanke, Phys. Rev. B **62**, 4336 (2000).
[27] J. Kokalj and P. Prelovšek, Eur. Phys. J. B **63**, 431 (2008).
[28] J. Ortloff, M. Balzer, and M. Potthoff, Eur. Phys. J. B **58**, 37 (2007).
[29] A. Georges, G. Kotliar, W. Krauth, and M. J. Rozenberg, Rev. Mod. Phys. **68**, 13 (1996).
[30] G. Kotliar, S. Y. Savrasov, K. Haule, V. S. Oudovenko, O. Parcollet, and C. A. Marianetti, Rev. Mod. Phys. **78**, 865 (2006).
[31] P. Limelette, A. Georges, D. Jérome, P. Wzietek, P. Metcalf, and J. Honig, Science **302**, 89 (2003).
[32] S. Tsuda, C. L. Yang, Y. Shimura, K. Umeo, H. Fukuoka, Y. Yamane, T. Onimaru, T. Takabatake, N. Kikugawa, T. Terashima, H. T. Hirose, S. Uji, S. Kittaka, and T. Sakakibara, Phys. Rev. B **98**, 155147 (2018).
[33] J. Shin, Z. Schlesinger, and B. S. Shastry, Phys. Rev. B **95**, 205140 (2017).
[34] A. E. Sikkema, W. J. L. Buyers, I. Affleck, and J. Gan, Phys. Rev. B **54**, 9322 (1996).
[35] W.-W. Yang, J.-Z. Zhao, H.-G. Luo, and Y. Zhong, Phys. Rev. B **100**, 045148 (2019).
[36] M. M. Maśka and K. Czajka, Phys. Rev. B **74**, 035109 (2006).
[37] See Supplemental Material at http://link.aps.org/supplemental/10.1103/PhysRevB.104.165146 for details of the phase diagram

in the $\mu - T$ plane, the DMFT study about the Mott criticality, the magnetic states at low-T, the characteristics of NFL-I and NFL-II, the resistivity around the crossover of NFL-I and SM state, and the finite size effect of violation of Luttinger theorem.

[38] C. M. Varma, Rep. Prog. Phys. **79**, 082501 (2016).

[39] C. M. Varma, Rev. Mod. Phys. **92**, 031001 (2020).

[40] I. M. Hayes, R. D. McDonald, N. P. Breznay, T. Helm, P. J. W. Moll, M. Wartenbe, A. Shekhter, and J. G. Analytis, Nat. Phys. **12**, 916 (2016).

[41] S. A. Kivelson, E. Fradkin, and V. J. Emery, Nature **393**, 550 (1998).

[42] D. V. D. Marel, H. J. A. Molegraaf, J. Zaanen, Z. Nussinov, F. Carbone, A. Damascelli, H. Eisaki, M. Greven, P. H. Kes, and M. Li, Nature **425**, 271 (2003).

[43] J. Zaanen, Nature **430**, 512 (2004).

[44] C. M. Varma, P. B. Littlewood, S. Schmitt-Rink, E. Abrahams, and A. E. Ruckenstein, Phys. Rev. Lett. **63**, 1996 (1989).

[45] I. Dzyaloshinskii, Phys. Rev. B **68**, 085113 (2003).

[46] J. M. Luttinger and J. C. Ward, Phys. Rev. **118**, 1417 (1960).

[47] J. M. Luttinger, Phys. Rev. **119**, 1153 (1960).

[48] M. Oshikawa, Phys. Rev. Lett. **84**, 3370 (2000).

[49] P. W. Phillips, L. Yeo, and E. W. Huang, Nat. Phys. **16**, 1175 (2020).

[50] T. Kennedy and E. H. Lieb, Physica A **138**, 320 (1986).

[51] D. I. Khomskii, *Basic Aspects of the Quantum Theory of Solids* (Cambridge University Press, Cambridge, England, 2010).